Damage Identification of supporting structures with a Moving Sensory System

by

Zhu, X.Q.[1], Law, S.S. [2,3], Huang, L. [4] and Zhu, S.Y. [5]

Abstract: An innovative approach to identify local anomalies in a structural beam bridge with an instrumented vehicle moving as a sensory system across the bridge. Accelerations at both the axle and vehicle body are measured from which vehicle-bridge interaction force on the structure is determined. Local anomalies of the structure are estimated from this interaction force with the Newton's iterative method basing on the homotopy continuation method. Numerical results with the vehicle moving over simply supported or continuous beams show that the acceleration responses from the vehicle or the bridge structure are less sensitive to the local damages than the interaction force between the wheel and the structure. Effects of different movement patterns and moving speed of the vehicle are investigated, and the effect of measurement noise on the identified results is discussed. A heavier or slower vehicle has been shown to be less sensitive to measurement noise giving more accurate results.

[1] School of Computing, Engineering and Mathematics, Western Sydney University, Penrith, NSW 2751, Australia. Email: xinqun.zhu@westernsydney.edu.au
[2] School of Civil Engineering, Chongqing University, China. E-mail address: siu-seong.law@connect.polyu.hk
[3] Civil and Environment Engineering Department, Hong Kong Polytechnic University, Kowloon, Hunghum, Hong Kong, China. E-mail address: siu-seong.law@connect.polyu.hk
[4] Civil and Environment Engineering Department, Hong Kong Polytechnic University, Kowloon, Hunghum, Hong Kong, China. E-mail address: 806045267@qq.com
[5] Civil and Environment Engineering Department, Hong Kong Polytechnic University, Kowloon, Hunghum, Hong Kong, China. E-mail address: ceszhu@polyu.edu.hk

Keywords: moving sensor; damage identification; homotopy iteration algorithm; interaction force

1 Introduction

The non-destructive approach for identifying local damages in a structure has been a hot research topic in the past few decades. Most literatures in this area are based on the characteristic dynamic parameters and responses [1] of structures. Sensors are often installed on the bridge deck for direct measurement of the responses of structure under load. Since the local damages are not known, a dense array of sensors should be used at different positions of the structure in practice to estimate the location and extent of the structural damage. Incorrect identification may occur when the sensor is far away from the local damage as local responses are sensitive to local damages. This phenomenom will be illustrated in Section 4.2.1 of this paper. Also, the design life of structure is usually much longer than the reliable lifespan of most sensors. The centralized long-term monitoring system requires costly onsite sensor maintenance due to the harsh operational environments. There is also a large stock of short and medium bridges, and most of them do not have such a system in practice. These form the main obstacles for general application of most existing damage detection algorithms.

Sensors have been installed on the axle or the vehicle body instead of the bridge deck [2,3] to enable the vehicle to serve as both an exciter and a sensory system. Yang et al. [4] extracted the natural frequencies of a bridge deck directly from accelerations obtained from the axle of a passing vehicle. The accelerometers and velocity meters were vertically installed near the center of the vehicle. Experimental verification has been conducted [5] using a four-wheel commercial light truck towing a small two-wheel cart. Two identical trailers were instrumented with sensors to capture the ambient vibration of the bridge, and the modal parameters are extracted by applying the short-time frequency domain decomposition [6] on the difference of signals from the two trailers. Yang and Chen [7] presented a method to identify the bridge natural frequencies from the dynamic response of a test vehicle using the stochastic subspace identification technique. Kong et al. [8] conducted field tests to extract bridge modal properties using a specialized test vehicle consisting of a tractor and two trailers. The tractor was used as the exciter and the trailers were instrumented with sensors. The responses of the trailers were used to extract the modal parameters of the bridge deck.

The above idea of a moving sensory system is for extracting the fundamental bridge frequency and mode shape. This indirect approach has also been adopted for damage detection in the last two decades. Bu et al. [9] proposed a method to assess the conditions of a bridge deck using

dynamic response of the passing vehicle with acceptable results. Kim and Kawatani [10] proposed a pseudo-static formulation of the vehicle-bridge interaction to identify the elemental stiffness changes of a bridge structure experimentally [11]. A truck-based mobile wireless sensory network has also been proposed to capture the vehicle-bridge interaction [12]. The wireless monitoring system is time-synchronized with the permanent wireless monitoring system installed on the bridge. Cerda et al. [13] collected data from passing vehicles over a bridge in an indirect approach of bridge health monitoring. The acceleration signals are wavelet decomposed. An instrumented truck-trailer vehicular system has been used to detect damping changes in a bridge deck with accelerometers fitted to the axles of the trailer [14,15]. Miyamoto and Yabe [16] studied the feasibility of the indirect approach to extract the bridge dynamic properties using an accelerometer mounted on the chassis of a public bus. The target bridge performance is evaluated from the measured acceleration data for the formulation of rational maintenance strategies. Zhang et al. [17] obtained damage information of a bridge deck using only one sensor mounted on a moving robot with a tapping device serving as an exciter. The operating deflection shape of the bridge deck was also estimated using information from a moving device [18], and its curvature can be obtained from wavelet-based filtering of the information for damage detection.

The above review shows that the use of a moving sensory system is feasible and reliable for damage identification. The moving sensory system proposed in this paper collects dynamic responses along its moving path and this is equivalent to measuring responses from a dense array of sensors along the structure. Local damage in a region trepassed by the vehicle can be accurately identified by the local responses collected. Accelerometers located on the axle and body of the moving vehicle collect the dynamic responses of the vehicle. The dynamic interaction force between the vehicle and structure can then be determined from these responses.

The identification equations from the above methods are usually solved iteratively in the inverse analysis using regularization method [9]. This and other method of optimization are locally convergent depending on the initial values. There are, however, algorithms for solving nonlinear sets of equation that are globally convergent without this constraint. The essence of these algorithms is the construction of an appropriate homotopy map and the tracking of solution sets on curves in this homotopy map. He [19] developed a new homotopy perturbation technique from the traditional perturbation method for solving different linear and nonlinear problems. Liao [20] proposed a homotopy analysis method which is capable to solve problems with highly nonlinear systems.

Alexander and Yorke [21] developed a homotopy continuation method to solve bifurcations problems in nonlinear systems with fixed points and singularities in the vector fields.

In this paper, the homotopy map in the damage detection problem studied is formulated according to the general homotopy method [19-21]. The solution of the homotopy equation is based on the homotopy continuation method [21]. However, successful solution of the homotopy equation depends on the smooth tracking of the solution in the homotopy path. Choi et al. [22] have employed both the Euler method and Newton method to track the solution. Both approaches do not perform well in the system identification of a structure due to the presence of a singular matrix resulting in a set of non-realistic result. Other researchers [23] estimated the homotopy parameter from the homotopy equation with improved solution in the homotopy path using Newton iterative method. The Newton's iterative method is adopted to track the correct solution path in this study. The proposed method of analysis based on interaction force has been shown to yield more accurate identified result than the regularization technique based on vehicle responses [9]. The interaction force under the wheel is shown much more sensitive to local damages in the structure than measured accelerations from either the structure or the moving vehicle. Different patterns of vehicle movement on deck, vehicle speed and measurement noise level on the identification are numerically investigated.

2 Theory

2.1 Determination of interaction force from vehicle responses

The moving vehicle is modeled as a five-parameter two degrees-of-freedom (DOFs) system as shown in Figure 1. It moves on the beam bridge at a uniform speed v from left to right. Two accelerometers are installed on the axle and body of the vehicle to collect the responses of the two masses. The physical properties of the vehicle are: an upper mass m_{v1} of the suspension, a lower mass m_{v2} of the bogie and axle connected to the suspension damper c_v and a suspension spring k_{v1}, together with another spring k_{v2} to model the stiffness of the tire. The equation of motion of the vehicle can be written as

$$m_{v1}\ddot{y}_1 + c_v(\dot{y}_1 - \dot{y}_2) + k_{v1}(y_1 - y_2) = 0 \tag{1}$$

$$m_{v2}\ddot{y}_2 + c_v(\dot{y}_2 - \dot{y}_1) + k_{v1}(y_2 - y_1) + k_{v2}(y_2 - y(x(t)) - r(x(t))) = 0 \tag{2}$$

where y_1 and y_2 are the displacement responses of the masses m_{v1} and m_{v2}, respectively. $y(x(t))$ is the displacement response of the bridge, $r(x(t))$ is the road surface roughness, and $x(t) = vt$ is the location of the vehicle on the deck at time instant *t*. The interaction force $P_{\text{int}}(t)$ between the bridge and the vehicle can be expressed as

$$P_{\text{int}}(t) = (m_{v1} + m_{v2})g + k_{v2}(y_2 - y(x(t)) - r(x(t))) \tag{3}$$

Substituting Eqs. (1) and (2) into Eq. (3), the interaction force can be rewritten as

$$P_{\text{int}}(t) = (m_{v1} + m_{v2})g - m_{v1}\ddot{y}_1 - m_{v2}\ddot{y}_2 \tag{4}$$

where the responses $\ddot{y}_1$ and $\ddot{y}_2$ are collected by the accelerometers. Combining Eqs. (1), (2) and (4), we have

$$\begin{bmatrix} m_{v1} & 0 \\ 0 & m_{v2} \end{bmatrix} \begin{Bmatrix} \ddot{y}_1 \\ \ddot{y}_2 \end{Bmatrix} + \begin{bmatrix} c_v & -c_v \\ -c_v & c_v \end{bmatrix} \begin{Bmatrix} \dot{y}_1 \\ \dot{y}_2 \end{Bmatrix} + \begin{bmatrix} k_{v1} & -k_{v1} \\ -k_{v1} & k_{v1} \end{bmatrix} \begin{Bmatrix} y_1 \\ y_2 \end{Bmatrix} = \begin{bmatrix} 0 \\ (m_{v1} + m_{v2})g - P_{\text{int}}(t) \end{bmatrix} \tag{5}$$

Let $\mathbf{M}_v = \begin{bmatrix} m_{v1} & 0 \\ 0 & m_{v2} \end{bmatrix}$, $\mathbf{C}_v = \begin{bmatrix} c_v & -c_v \\ -c_v & c_v \end{bmatrix}$, $\mathbf{K}_v = \begin{bmatrix} k_{v1} & -k_{v1} \\ -k_{v1} & k_{v1} \end{bmatrix}$, $\mathbf{y}_v = \begin{Bmatrix} y_1 \\ y_2 \end{Bmatrix}$, $F_v = (m_{v1} + m_{v2})g$, Eq. (5) can be rewritten as

$$\mathbf{M}_v\ddot{\mathbf{y}}_v + \mathbf{C}_v\dot{\mathbf{y}}_v + \mathbf{K}_v\mathbf{y}_v = \mathbf{D}(F_v - P_{\text{int}}(t)) \tag{6}$$

where $\mathbf{D} = \begin{bmatrix} 0 & 1 \end{bmatrix}^T$ is the mapping vector.

2.2 Damage identification from the Interaction force

The beam bridge shown in Figure 1 has span length L and it is modeled as a planar Euler-Bernoulli beam with *n* finite elements. The equation of motion of the bridge can be expressed as

$$\mathbf{M}_b\ddot{\mathbf{y}}_b(t) + \mathbf{C}_b\dot{\mathbf{y}}_b(t) + \mathbf{K}_b\mathbf{y}_b(t) = \mathbf{R}^T(t)P_{\text{int}}(t) \tag{7}$$

where $\mathbf{M}_b$, $\mathbf{C}_b$ and $\mathbf{K}_b$ are the mass, damping and stiffness matrices of the structure respectively. Rayleigh damping $\mathbf{C}_b = a_1\mathbf{M}_b + a_2\mathbf{K}_b$ is assumed, where a_1 and a_2 are the two Rayleigh damping coefficients. $\ddot{\mathbf{y}}_b$, $\dot{\mathbf{y}}_b$ and $\mathbf{y_b}$ are respectively the acceleration, velocity and displacement response vectors of the bridge. Note that the function *(t)* has been omitted for convenience.

$\mathbf{R}(t) = \{0, 0, \cdots, \mathbf{R}_i(t), \cdots, 0\}$ is a function of time and $\mathbf{R}_i(t)$ is the vector of shape functions in the *i*th element on which the moving sensor is located at time instant *t*, and this can be expressed as

$$\mathbf{R}_i(t) = \left\{1 - 3\xi^2 + 2\xi, (\xi - 2\xi^2 + \xi^3)l_e, 3\xi^2 - 2\xi^3, (-\xi^2 + \xi^3)l_e\right\}$$

with $\xi = (x(t) - x_i)/l_e$, and $x_i = (i-1)l_e$, and l_e is the length of the element.

The acceleration, velocity and displacement responses of the time invariant system in *y*-direction in Eq. (7) can be written as

$$\ddot{y}_b(x(t)) = \mathbf{R}^a(t)\ddot{\mathbf{y}}_b(t) \tag{8a}$$

$$\dot{y}_b(x(t)) = \mathbf{R}^v(t)\dot{\mathbf{y}}_b(t) \tag{8b}$$

$$y_b(x(t)) = \mathbf{R}^d(t)\mathbf{y}_b(t) \tag{8c}$$

where $\mathbf{R}^a(t), \mathbf{R}^v(t)$ and $\mathbf{R}^d(t)$ are the output influence matrices for the "measured" acceleration, velocity and displacement, respectively. They form the mapping matrix $\mathbf{R}(t)$ when considering the entire time history.

Combining Eqs. (4), (6), (7) and (8), the coupled equation of motion of both the vehicle and structure can be written as

$$\mathbf{M}\ddot{\mathbf{Y}}(t) + \mathbf{C}\dot{\mathbf{Y}}(t) + \mathbf{K}\mathbf{Y}(t) = \mathbf{F}(t) \tag{9}$$

where $\mathbf{M} = \begin{bmatrix} \mathbf{M}_b & \mathbf{R}^T(t)m_{v1} & \mathbf{R}^T(t)m_{v2} \\ 0 & m_{v1} & 0 \\ 0 & 0 & m_{v2} \end{bmatrix}$, $\mathbf{C} = \begin{bmatrix} \mathbf{C}_b & 0 & 0 \\ 0 & c_v & -c_v \\ 0 & -c_v & c_v \end{bmatrix}$, $\mathbf{K} = \begin{bmatrix} \mathbf{K}_b & 0 & 0 \\ 0 & k_{v1} & -k_{v1} \\ -\mathbf{R}(t)k_{v2} & -k_{v1} & k_{v1} + k_{v2} \end{bmatrix}$,

$\mathbf{Y}(t) = \begin{Bmatrix} \mathbf{y}_b(t) \\ y_1(t) \\ y_2(t) \end{Bmatrix}$ and $\mathbf{F}(t) = \begin{bmatrix} \mathbf{R}^T(t)(m_{v1} + m_{v2}) \\ 0 \\ k_{v2}r(x(t)) \end{bmatrix}$.

3 Damage detection algorithms

3.1 Damage model

The beam bridge is assumed to remain linear-elastic and isotropic after damage occurrence. A simple damage model is adopted in this paper where the local damage is modeled as a reduction in the elemental flexural stiffness. The elemental flexural stiffness of a damaged element can be

expressed as

$$(EI)_i = (1-\alpha_i)(EI)_i^0,\ (i=1,2,\cdots,n) \tag{10}$$

where $(EI)_i^0$ is the ith elemental flexural stiffness in the intact state. α_i represents the reduction coefficient of the elemental flexural stiffness in the ith element, and it is called the stiffness parameter or damage parameter with $0 \le \alpha_i \le 1.0$.

3.2 Objective Function and Identification Equation

The damage detection of a structure can be considered as an optimization problem to find the vector of stiffness parameters $\boldsymbol{\alpha} = (\alpha_1, \alpha_2, \cdots, \alpha_n)^T$. The error between the computational and the measured values can be written as

$$J(\boldsymbol{\alpha}) = \frac{1}{2}\sum_{j=1}^{nt}\left(\boldsymbol{Q}_c(\boldsymbol{\alpha},t) - \boldsymbol{Q}_m(\boldsymbol{\alpha},t)\right)^2,\ \ (j=1,2,\cdots,nt) \tag{11}$$

where $\boldsymbol{Q}_c$ and $\boldsymbol{Q}_m$ are the computed response function and the measured response function with respect to the stiffness parameters, respectively. Variable t denotes the time instants; dt is the time step increment, and $nt = t/dt$ is the number of time step,

Three different response functions are considered here for comparison, viz, acceleration response of the vehicle, acceleration response of the beam bridge and the interaction force of the system. The acceleration response of the vehicle and bridge can be obtained from Eq. (9) with information of the vehicle. The interaction force can be derived from Eq. (4). Taking partial derivative of Eq. (11) with respect to the stiffness parameters, we have

$$f(\boldsymbol{\alpha}) = \begin{bmatrix} \sum_{j=1}^{nt}\left(\boldsymbol{Q}_c(\boldsymbol{\alpha},t) - \boldsymbol{Q}_m(\boldsymbol{\alpha},t)\right)\dfrac{\partial \boldsymbol{Q}_c(\boldsymbol{\alpha},t)}{\partial \alpha_1} \\ \sum_{j=1}^{nt}\left(\boldsymbol{Q}_c(\boldsymbol{\alpha},t) - \boldsymbol{Q}_m(\boldsymbol{\alpha},t)\right)\dfrac{\partial \boldsymbol{Q}_c(\boldsymbol{\alpha},t)}{\partial \alpha_2} \\ \vdots \\ \sum_{j=1}^{nt}\left(\boldsymbol{Q}_c(\boldsymbol{\alpha},t) - \boldsymbol{Q}_m(\boldsymbol{\alpha},t)\right)\dfrac{\partial \boldsymbol{Q}_c(\boldsymbol{\alpha},t)}{\partial \alpha_n} \end{bmatrix} \tag{12}$$

where $\dfrac{\partial \boldsymbol{Q}_c(\boldsymbol{\alpha},t)}{\partial \alpha_i}$ is the response sensitivity that is the first partial derivative of the computed

response with respect to the stiffness parameters. If $\boldsymbol{Q}_c$ is the acceleration response, $\frac{\partial \ddot{\mathbf{y}}_1(t)}{\partial \alpha_i}$, $\frac{\partial \ddot{\mathbf{y}}_2(t)}{\partial \alpha_i}$ and $\frac{\partial \ddot{\mathbf{y}}_b(t)}{\partial \alpha_i}$denote the acceleration response sensitivities that are the first partial derivative of the acceleration responses of the vehicle and the beam bridge respectively. They can be numerically obtained from taking the first partial derivative of Eq. (9) with respect to the stiffness parameters and then solving the equations obtained using Newmark integration method [24].

If $\boldsymbol{Q}_c$ is the interaction force, the first derivative of Eq. (7) with respect to the stiffness parameter can be written as

$$\mathbf{M}_b \frac{\partial \ddot{\mathbf{y}}_b(t)}{\partial \alpha_i} + \mathbf{C}_b \frac{\partial \dot{\mathbf{y}}_b(t)}{\partial \alpha_i} + \mathbf{K}_b \frac{\partial \mathbf{y}_b(t)}{\partial \alpha_i} + a_2 \frac{\partial \mathbf{K}_b}{\partial \alpha_i} \dot{\mathbf{y}}_b(t) + \frac{\partial \mathbf{K}_b}{\partial \alpha_i} \mathbf{y}_b(t) = \mathbf{R}^T(t) \frac{\partial \boldsymbol{Q}_c(t)}{\partial \alpha_i} \tag{13}$$

Thus the sensitivity of the interaction force can be derived as the first partial derivative of the interaction force $\frac{\partial \boldsymbol{Q}_c(\boldsymbol{\alpha},t)}{\partial \alpha_i} = \frac{\partial \mathbf{P}_{\text{int}}(\boldsymbol{\alpha},t)}{\partial \alpha_i}$ from Eq. (13)

$$\frac{\partial \boldsymbol{Q}_c(\boldsymbol{\alpha},t)}{\partial \alpha_i} = (\mathbf{R}^T(t)\mathbf{R}(t))^{-1}\mathbf{R}^T(t)\left(\mathbf{M}_b \frac{\partial \ddot{\mathbf{y}}_b(t)}{\partial \alpha_i} + \mathbf{C}_b \frac{\partial \dot{\mathbf{y}}_b(t)}{\partial \alpha_i} + \mathbf{K}_b \frac{\partial \mathbf{y}_b(t)}{\partial \alpha_i} + a_2 \frac{\partial \mathbf{K}_b}{\partial \alpha_i} \dot{\mathbf{y}}_b(t) + \frac{\partial \mathbf{K}_b}{\partial \alpha_i} \mathbf{y}_b(t)\right) \tag{14}$$

3.3 Homotopy Continuation Algorithm

The homotopy continuation algorithm [21-23] introduces a homotopy parameter λ with $\lambda \in [0,1]$ into the function $f(\boldsymbol{\alpha})$ in Eq. (12) to construct a family of homotopy mapping $H(\boldsymbol{\alpha},\lambda)=0$. The homotopy equation for the present problem takes up the following form as

$$H(\boldsymbol{\alpha},\lambda) = \lambda f(\boldsymbol{\alpha}) + (1-\lambda) g(\boldsymbol{\alpha}) = 0 \tag{15}$$

where function $g(\boldsymbol{\alpha})$ is related to the vector of arbitrarily selected initial values $\boldsymbol{\alpha}_0$, and it is assumed to have a form similar to $f(\boldsymbol{\alpha})$ with $g(\boldsymbol{\alpha}) = \sum_{j=1}^{nt} \left(\boldsymbol{Q}_c(\boldsymbol{\alpha},t) - \boldsymbol{Q}_c(\boldsymbol{\alpha}_0,t)\right) \frac{\partial \boldsymbol{Q}_c(\boldsymbol{\alpha},t)}{\partial \boldsymbol{\alpha}}$.

In the homotopy continuation algorithm, the homotopy parameter has a range $\lambda \in [0,1]$ and it is divided into *N* sub-intervals. Solution in each sub-interval is obtained by the Newton iterative method for updating the stiffness parameters and the homotopy equation. There are *N+1* homotopy equations for the *N* sub-intervals with $\lambda = 0, 1/\mathrm{N}, \cdots, 1$. A family of homotopy mapping $H(\boldsymbol{\alpha},\lambda) = 0$ is constructed instead of a single mapping. Eq. (15) can be rewritten as

$H(\boldsymbol{\alpha},0)=g(\boldsymbol{\alpha})=0$ when the homotopy parameter is zero, i.e. the arbitrarily selected initial point of the homotopy path is the starting point for the iteration. When the homotopy parameter increases to unity, the homotopy equation becomes $H(\boldsymbol{\alpha},1)=f(\boldsymbol{\alpha})=0$ where the solution matches the objective function.

The Newton's iterative method tracks and updates the vector of stiffness parameters, $\boldsymbol{\alpha}^{s+1}$, in the homotopy path in each sub-interval of the homotopy parameter as

$$\boldsymbol{\alpha}^{s+1}=\boldsymbol{\alpha}^{s}-\left(\frac{\partial H(\boldsymbol{\alpha},\lambda^{s+1})}{\partial\boldsymbol{\alpha}}\bigg|_{\boldsymbol{\alpha}=\boldsymbol{\alpha}^{s}}\right)^{-1}H(\boldsymbol{\alpha}^{s},\lambda^{s+1}) \tag{16}$$

where $\boldsymbol{\alpha}^{s}$ is the vector of stiffness parameters in the *sth* iterative step. $\frac{\partial H(\boldsymbol{\alpha},\lambda^{s+1})}{\partial\boldsymbol{\alpha}}$ is the first derivative of H with respective to the damage parameters when the value of homotopy parameter is λ^{s+1}, and it can be obtained from Eq.(15) as

$$\frac{\partial H(\boldsymbol{\alpha},\lambda^{s+1})}{\partial\boldsymbol{\alpha}}=\lambda^{s+1}\frac{\partial f(\boldsymbol{\alpha})}{\partial\boldsymbol{\alpha}}+(1-\lambda^{s+1})\frac{\partial g(\boldsymbol{\alpha})}{\partial\boldsymbol{\alpha}} \tag{17}$$

with $\dfrac{\partial f(\boldsymbol{\alpha})}{\partial\boldsymbol{\alpha}}=\left[\sum_{j=1}^{nt}\left(\left(\mathbf{Q}_c(\boldsymbol{\alpha},t)-\mathbf{Q}_m(\boldsymbol{\alpha},t)\right)\frac{\partial\mathbf{Q}_c^2(\boldsymbol{\alpha},t)}{\partial\alpha_i\partial\alpha_k}+\frac{\partial\mathbf{Q}_c(\boldsymbol{\alpha},t)}{\partial\alpha_k}\frac{\partial\mathbf{Q}_c(\boldsymbol{\alpha},t)}{\partial\alpha_i}\right),\quad (i,k=1,2,\cdots,n)\right]$

and $\dfrac{\partial g(\boldsymbol{\alpha})}{\partial\boldsymbol{\alpha}}=\left[\sum_{j=1}^{nt}\left(\left(\mathbf{Q}_c(\boldsymbol{\alpha},t)-\mathbf{Q}_c(\boldsymbol{\alpha}_0,t)\right)\frac{\partial\mathbf{Q}_c^2(\boldsymbol{\alpha},t)}{\partial\alpha_i\partial\alpha_k}+\frac{\partial\mathbf{Q}_c(\boldsymbol{\alpha},t)}{\partial\alpha_k}\frac{\partial\mathbf{Q}_c(\boldsymbol{\alpha},t)}{\partial\alpha_i}\right),\quad (i,k=1,2,\cdots,n)\right]$

and $\frac{\partial\boldsymbol{Q}_c^2(\boldsymbol{\alpha},t)}{\partial\alpha_i\partial\alpha_k}$ is the second partial derivative of the response function with respect to the stiffness parameters. The subscripts i and k are the element number.

If $\boldsymbol{Q}_c$ is the acceleration response, the second partial derivative of the acceleration responses $\frac{\partial\ddot{\mathbf{y}}_1^2(t)}{\partial\alpha_i^2}$, $\frac{\partial\ddot{\mathbf{y}}_2^2(t)}{\partial\alpha_i^2}$ and $\frac{\partial\ddot{\mathbf{y}}_n^2(t)}{\partial\alpha_i^2}$ can be obtained by taking the second derivative of Eq. (9) with respect to the stiffness parameters as

$$
\begin{cases}
\mathbf{M}\dfrac{\partial^2 \boldsymbol{Q}_c(t)}{\partial \alpha_i^2}+\mathbf{C}\dfrac{\partial^2 \dot{\mathbf{Y}}(t)}{\partial \alpha_i^2}+\mathbf{K}\dfrac{\partial^2 \mathbf{Y}(t)}{\partial \alpha_i^2}=-a_2\dfrac{\partial \mathbf{K}}{\partial \alpha_i}\dfrac{\partial \dot{\mathbf{Y}}(t)}{\partial \alpha_i}-\dfrac{\partial \mathbf{K}}{\partial \alpha_i}\dfrac{\partial \mathbf{Y}(t)}{\partial \alpha_i}-a_2\dfrac{\partial^2 \mathbf{K}}{\partial \alpha_i^2}\dot{\mathbf{Y}}(t)-\dfrac{\partial^2 \mathbf{K}}{\partial \alpha_i^2}\mathbf{Y}(t) \\
\mathbf{M}\dfrac{\partial^2 \boldsymbol{Q}_c(t)}{\partial \alpha_i \partial \alpha_k}+\mathbf{C}\dfrac{\partial^2 \dot{\mathbf{Y}}(t)}{\partial \alpha_i \partial \alpha_k}+\mathbf{K}\dfrac{\partial^2 \mathbf{Y}(t)}{\partial \alpha_i \partial \alpha_k}=-a_2\dfrac{\partial \mathbf{K}}{\partial \alpha_k}\dfrac{\partial \dot{\mathbf{Y}}(t)}{\partial \alpha_i}-\dfrac{\partial \mathbf{K}}{\partial \alpha_k}\dfrac{\partial \mathbf{Y}(t)}{\partial \alpha_i}-a_2\dfrac{\partial^2 \mathbf{K}}{\partial \alpha_i \partial \alpha_k}\dot{\mathbf{Y}}(t)-\dfrac{\partial^2 \mathbf{K}}{\partial \alpha_i \partial \alpha_k}\mathbf{Y}(t) \\
\mathbf{M}\dfrac{\partial^2 \boldsymbol{Q}_c(t)}{\partial \alpha_k \partial \alpha_i}+\mathbf{C}\dfrac{\partial^2 \dot{\mathbf{Y}}(t)}{\partial \alpha_k \partial \alpha_i}+\mathbf{K}\dfrac{\partial^2 \mathbf{Y}(t)}{\partial \alpha_k \partial \alpha_i}=-a_2\dfrac{\partial \mathbf{K}}{\partial \alpha_i}\dfrac{\partial \dot{\mathbf{Y}}(t)}{\partial \alpha_k}-\dfrac{\partial \mathbf{K}}{\partial \alpha_i}\dfrac{\partial \mathbf{Y}(t)}{\partial \alpha_k}-a_2\dfrac{\partial^2 \mathbf{K}}{\partial \alpha_k \partial \alpha_i}\dot{\mathbf{Y}}(t)-\dfrac{\partial^2 \mathbf{K}}{\partial \alpha_k \partial \alpha_i}\mathbf{Y}(t) \\
\mathbf{M}\dfrac{\partial^2 \boldsymbol{Q}_c(t)}{\partial \alpha_k^2}+\mathbf{C}\dfrac{\partial^2 \dot{\mathbf{Y}}(t)}{\partial \alpha_k^2}+\mathbf{K}\dfrac{\partial^2 \mathbf{Y}(t)}{\partial \alpha_k^2}=-a_2\dfrac{\partial \mathbf{K}}{\partial \alpha_k}\dfrac{\partial \dot{\mathbf{Y}}(t)}{\partial \alpha_k}-\dfrac{\partial \mathbf{K}}{\partial \alpha_k}\dfrac{\partial \mathbf{Y}(t)}{\partial \alpha_k}-a_2\dfrac{\partial^2 \mathbf{K}}{\partial \alpha_k^2}\dot{\mathbf{Y}}(t)-\dfrac{\partial^2 \mathbf{K}}{\partial \alpha_k^2}\mathbf{Y}(t)
\end{cases}
\tag{18}
$$

where $\dfrac{\partial \boldsymbol{Q}_c{}^2(t)}{\partial \alpha_i \partial \alpha_k}=\left[\dfrac{\partial \boldsymbol{y}_b^2(t)}{\partial \alpha_i \partial \alpha_k},\dfrac{\partial y_1^2(t)}{\partial \alpha_i \partial \alpha_k},\dfrac{\partial y_2^2(t)}{\partial \alpha_i \partial \alpha_k}\right]^T$, and Eq. (18) using Newmark integration method.

If $\boldsymbol{Q}_c$ is the interaction force, the term $\dfrac{\partial \boldsymbol{Q}_c^2(\boldsymbol{\alpha},t)}{\partial \alpha_i \partial \alpha_k}$ can be similarly obtained by taking the second derivative of Eq. (7) with respect to the stiffness parameters and solve the equation using Newmark integration method.

In the Newton's iteration algorithm, the criterion of convergence is defined as

$$
\frac{\left\|(\boldsymbol{EI})^{s+1}-(\boldsymbol{EI})^{s}\right\|}{\left\|(\boldsymbol{EI})^{s+1}\right\|}\le Tol1 \tag{19a}
$$

where *Tol1* is a small convergence threshold. The solution is also required to satisfy Eq. (19b) as shown below.

$$
\left\|H(\boldsymbol{\alpha}^{s+1},\lambda^{s+1})\right\|\le Tol2 \tag{19b}
$$

where *Tol2* is a small value close to zero. *Tol1* and *Tol2* are taken equal to 1.0×10^{-4} and 10.0 in this work unless otherwise stated.

The present study shows that the solution satisfying either Eq. (19b) or Eq. (19a) are close to each other (computation in Section 4.1.2 is referred). The updated point on the homotopy path satisfying Eq. (19a) is considered also satisfying Eq. (19b), and the second convergence criterion in Eq. (19b) is therefore neglected for a faster computation.

3.4 Implementation procedure

The computation procedure can be implemented as follows:

Step 1: Collect the acceleration responses of the vehicle.

Step 2: Provide a good guess on the vector of initial damage parameters $\boldsymbol{\alpha}_0$, and let $\boldsymbol{\alpha}^s = \boldsymbol{\alpha}_0$ (s=0) with s denotes the iteration number. The homotopy parameter taking up the range of $\lambda \in [0,1]$ is divided into N equal parts with $d\lambda = 1/\mathrm{N}$. Then let λ^s =0 (s=0). The vector of initial values is set equal to null in this work.

Step 3: Trace solution in the homotopy path starting from the initial value (α^0, λ^0) as follows. Apply an increment to the homotopy parameter λ^s as, $\lambda^{s+1} = \lambda^s + d\lambda$.

Step 4: Calculate the dynamic responses of the vehicle and the interaction force under the wheel from Eqs. (4), (9) and (10) from initial models of the structure and the vehicle. Obtain the homotopy equation from Eqs. (12) and (15).

Step 5: Use Newton's iterative method to update the damage parameter vector $\boldsymbol{\alpha}^{s+1}$ at a point along the homotopy path from Eqs. (16) and (17).

Step 6: Check whether the damage vector $\boldsymbol{\alpha}^{s+1}$ obtained has any physical meaning, i.e. when $\alpha_i^{s+1} > 1.0$, the stiffness parameter loses its physical significance. If yes, go to Step 7. Otherwise, the result is considered diverged, and either separate the range of homotopy parameter into more divisions or a new set of initial values is assigned. Then go to Step 2.

Step 7: Let $\boldsymbol{\alpha}^s = \boldsymbol{\alpha}^{s+1}$ and $(\boldsymbol{EI})^s = (\boldsymbol{EI})^{s+1}$, and repeat Steps 4 to 6 until the obtained (α^{s+1}, λ^{s+1}) and $(\boldsymbol{EI})^{s+1}$ in the homotopy path satisfies the convergence criterion in Eqs. (19a) and (19b).

Step 8: The set of initial values is updated with (α^{s+1}, λ^{s+1}) obtained in last step. Repeat Steps 3 to 7 for the whole range of the homotopy parameter λ^{r+1}. The final set of α^{s+1} obtained is the corresponding updated set of stiffness parameters.

4 Numerical simulations

4.1 Verification of the proposed method

The bridge-vehicle system studied by Bu et al. [9] is investigated for comparison. The properties of the simply supported beam bridge are: $L = 30m$, $EI = 2.5\times10^{10} N\cdot m^2$, $\rho A = 6.0\times10^3 kg/m$, and the damping coefficients $a_1 = 0.343$ and $a_2 = 0.001$ are respectively. The parameters of the vehicle are: $m_{v1} = 3.6\times10^3 kg$, $m_{v2} = 0.25\times10^3 kg$, $c_v = 1.0\times10^3 Ns/m$, $k_{v1} = 6.0\times10^5 N/m$ and $k_{v2} = 8.5\times10^5 N/m$. The simply supported deck is discretized into 10 equal Euler-Bernoulli beam

elements, and the sampling frequency is 200Hz. The sampling rate would be sufficient to accommodate the natural frequencies of the vehicle which are 1.6 Hz and 12.2 Hz as well the first three natural frequencies 3.6Hz, 14.3Hz and 32.1Hz of the structure in the simulation studies. The speed of the vehicle is set at 20m/s as in Bu et al. [9] and it moves on the beam with Class C road surface roughness [25].

4.1.1 Comparison of different types of sensitivities to local damages

The sensitivity of the interaction force underneath the moving vehicle is compared with the sensitivity of responses from the vehicle and from the beam bridge in this study. The vertical acceleration responses from the vehicle axle mass m_{v1}, the body mass m_{v2} and from Node 4 on the bridge beam are calculated as the "measured" responses with the passage of the vehicle. The sensitivity of these responses with respect to a local change in the stiffness parameter in Elements 1, 2, 4 and 6 are computed. The sensitivity of the interaction force is also computed. The three types of sensitivity time histories are shown in Figure 2. The acceleration response of structure is found much less sensitive to the local damaged element than the interaction force under the wheel. The axle acceleration response of the vehicle is found more sensitive to these local damages than response from the vehicle body.

4.1.2 Comparison of identified results from different types of sensitivities

The same beam bridge and vehicle as for last study are adopted. Multiple local damages are simulated with a reduction of the stiffness parameter by 5%, 10%, 10% and 15% in Elements 1, 2, 4 and 6 respectively. There are two divisions in the homotopy parameter. An absolute error (AE) is defined to compare the accuracy of the identification as

$$\mathrm{AE} = \left\| \boldsymbol{\alpha}^{true} - \boldsymbol{\alpha}^{identified} \right\| \tag{20}$$

where $\|\bullet\|$ is the norm of the vector. $\boldsymbol{\alpha}^{true}$ is the true vector of stiffness parameters; $\boldsymbol{\alpha}^{identified}$ is the vector of the final identified stiffness parameters.

Identified results from different responses are shown in Table 1. Accurate result can be obtained by using the interaction force and different types of acceleration responses. Results from using the interaction force are more accurate with less iteration in computation because it is more sensitive to local damages than the accelerations. Also, slightly better results can be obtained from using the acceleration responses in the homotopy iteration algorithm compared to the sensitivity method in Bu et al [9].

It may be concluded that different acceleration responses can be used to identify the local damage successfully but not that accurate as those from the interaction force. Therefore, only the interaction force will be adopted for the remaining studies in this paper.

The evolution of the identified results from the interaction force is shown in Figure 3. "Ele4" is the abbreviation of “Element 4”. Since there are two divisions in the homotopy parameter, the result converges twice in the computation process at 30th iteration when the homotopy parameter is 0.5, and again at the 55th iteration when the homotopy parameter is unity. The final updated results are very close to the real stiffness parameters of the structure. Results in Figure 3(a) satisfy the convergence requirement in Eq. (19a), while those in Figures 3(b) satisfy both convergence requirements in Eqs. (19a) and (19b) from a separate study. The two sets of identified results are similar and accurate, but the latter set has been obtained with more iterations. Hence, the second criterion in Eq. (19b) is ignored in the remaining studies for a faster computation.

4.2 Study 1: A two-span continuous beam

The effect of different influencing factors on the identification using the homotopy iteration algorithm will be studied. The two-span continuous beam shown in Figure 4 has the following properties: length $L = 15m$ for each span, elastic modulus $E = 34GPa$, mass density $\rho = 2800kg/m^3$, and the cross-section of the beam is $4m$ wide and $0.25m$ thick. The beam is discretized into 10 equal elements in each span with the element numbering system as shown. The same moving vehicle as for last study is adopted. Other parameters for the simulation are the same as for last study.

4.2.1 Effect of different moving patterns

Four different moving patterns of the vehicle are shown in Figure 5. The first one has the vehicle moves from the left end to the right end of the bridge at a constant speed of 4m/s. The second one has the vehicle moves with the same constant speed in the first 23.6 meters. Then the vehicle decelerates at 2.5m/s^2 until it stops at 26.8 meters from the left end. The other two patterns are similar to the second one but with the vehicle decelerating earlier at 6 meters and 15 meters from the left end, respectively. The same amount of data (1500 data) will be calculated as the “measured” data from sensors on the vehicle even when it stops in these three moving patterns for the subsequent identification. Only one local damage is simulated at Element 20 with 10% reduction in the stiffness parameter. The division of the homotopy parameter is kept at two.

The evolution of the identified results is shown in Figure 6. Since the damage is at the right end of the beam, only the first two patterns can identify the damage correctly. Results from pattern

four are poor and all the incorrectly identified results are in the second span. This is because the vehicle stops at 9.2 meters from the left end, and the interaction force for identification mainly comes from the first span of the deck, while the local damage is close to the end of the second span. This serves as an evidence that local damage should better be identified from using local measurements.

The vehicle in pattern three stops at 18.2 meters from the left end, and the incorrect identified result is in Element 19 next to Element 20 with a magnitude of 0.35.

The first moving pattern is noted to give good identified results with less computation (17 iterations) than in the other patterns. Since it is not easy to control deceleration of the vehicle in practice, the first movement pattern of the vehicle will be used for the following studies.

4.2.2 Effect of moving speed of the vehicle

The scenarios with the vehicle moves at a constant speed of 1m/s, 4m/s and 14m/s are studied. The last speed represents approximately 50 km/h. The sampling rate is kept at 200 Hz, while other parameters of the system are the same as those for last study. The local damage scenario for the last study is adopted. Cases without noise and with 2%, 5% and 10% noise in the acceleration response are studied. The measurement noise is normally distributed with zero mean and a unit standard deviation. The polluted responses is obtained by adding the noise vector to the calculated vehicle acceleration as

$$\begin{cases} \ddot{y}_1^{polluted} = \ddot{y}_1^{calculated} + E_p \times \mathbf{N}_{oise}^1 \times \mathrm{var}(\ddot{y}_1^{calculated}) \\ \ddot{y}_2^{polluted} = \ddot{y}_2^{calculated} + E_p \times \mathbf{N}_{oise}^2 \times \mathrm{var}(\ddot{y}_2^{calculated}) \end{cases} \tag{21}$$

where $\ddot{y}_1^{polluted}$ and $\ddot{y}_2^{polluted}$ are the vector of polluted "measured" acceleration response; $\ddot{y}_1^{calculated}$ and $\ddot{y}_2^{calculated}$ are the calculated acceleration response of the vehicle; E_P is the noise level; $\mathbf{N}_{oise}^1$ and $\mathbf{N}_{oise}^2$ are two different normal distribution vector with zero mean and unit standard deviation; $\mathrm{var}(\bullet)$ is the standard deviation of the calculated acceleration response. The polluted interaction force can also be obtained from Eq. (4) with the polluted "measured" acceleration responses for this study.

Two divisions in the homotopy parameter are adopted when there is no measurement noise. When there is noise in the measurement, 5 divisions and 15 divisions in the homotopy parameter are adopted for speeds of 1m/s and 4m/s and speed 14m/s, respectively to improve the convergence of the solution. The identification results are shown in Figure 7. The absolute error as calculated from

Eq. (20) and the iteration number required are presented in Table 2. Accurate identified result is noted when there is no noise in the measured responses. However, when measurement noise exists, incorrect identification occurs especially when the speed is 4m/s and 14m/s.

The sensitivities of interaction force with respect to damage in Element 20 for different moving speeds are shown in Figure 8. It is noted that a lower speed has much higher sensitivity to the damage element than a higher speed at 4m/s and 14m/s. This explains why the identification from lower travelling speed of the vehicle can yield more accurate identified result than from a higher speed when there is measurement noise effect.

4.2.3 Effect of sampling frequency

The identified result from last study is poor when the sampling frequency is 200Hz and the moving speed is 4m/s. This study is repeated in this Section with a sampling frequency of 500Hz and 1000Hz to check on the effect of a higher sampling rate. Other parameters are the same as for last study. The absolute error of identification and iteration required are shown in Table 2. Incorrect results are noted in the cases with noisy measurement, especially when there is 10% noise. The errors listed in Table 2 show that the accuracy of identification can be improved over the whole range of noise level studied with a higher sampling frequency.

4.2.4 Identification of multiple damages

Multiple damages in the structure are simulated with a reduction of 5%、10%、8%、12% and 10% of the stiffness parameter in Elements 1, 2, 7, 16 and 20 respectively. The moving speed is assumed to be 1m/s and the sampling frequency is 200Hz. Cases without noise and with 2%, 5% and 10% measurement noise are studied. There will be 10 divisions in the homotopy parameter. Other parameters are the same as for last study. The identified results are shown in Figure 9. Local damages can be identified satisfactory even with 10% measurement noise, with the largest false positive less than 2.5% at Element 15. The required number of iterations for the cases without noise and with 2%, 5% and 10% noise levels are 211, 188, 145 and 187 respectively.

It is noted that the computation converges faster when there is noise effect as noted above. A convergence threshold of 1.0×10^{-4} has been adopted as stated underneath Eq. (19b), and this is applicable to both cases with and without measurement noise effect. The Newton's iterative method has the converged results from the ith division serving as the initial values for optimization in the (i+1)th division of the homotopy parameter. It has also been stated that a finer division of the homotopy parameter would give better estimate on the unknown parameters for optimization in the next division. Ten divisions have been adopted in this study, and yet the convergence is slightly

faster when there is noise effect. This observation cannot be explained with the computation constraints adopted. This set of result may, however, due to the different noise vectors in each case as the trend of required iteration for convergence is not consistent with the noise level.

4.3 Study 2: A three-span continuous haunch beam

The proposed method is further verified with application to a more realistic three-span continuous haunch bridge [26] as shown in Figure 10. The properties of the beam bridge are: length $L = 60m$, elastic modulus $E = 30GPa$, mass density $\rho = 2400kg/m^3$, width of deck is $0.5m$, and the depth varies from $1m$ to $1.6m$ as shown. Each span of the beam is discretized into 10 equal length elements and there is a total of 30 Euler-Bernoulli beam finite elements in the structure. One vehicle moves from the left end to the right end of the bridge with a constant speed of 5m/s. The parameter m_{v1} of the vehicle body is set to be one, three or five times the weight of vehicle adopted in previous studies to study the effect of vehicle mass and they correspond to Scenarios 1, 2 and 3 respectively. The sampling rate of 200 Hz is adopted. Other parameters are the same as those for last study. Multiple damages are simulated with a reduction of 10%, 5%, 6% and 12% in Elements 1, 11, 20 and 30 respectively. This simulates the situation when local damages are located close to supports, and they are usually difficult to be identified with existing damage detection algorithms. Cases without noise and with 5% and 10% noise are studied.

The required number of iteration in computation and the number of divisions of the homotopy parameter are shown in Table 3. The identified results are shown in Figure 11. Accurate results can be obtained for all cases when there is no measurement noise. The location of the local damages can be identified correctly in all noisy cases, and the estimate of damage extent is poorer with higher measurement noise in general. The largest error is 2.58% in Element 13 and 2.18% in Element 13 with 10% noise in Scenarios 1 and 2 respectively. There are no notable false positives in Scenario 3 and all the errors are noted small to be ignored. Hence, it may be concluded that a heavier vehicle body could suppress significantly the measurement noise effect in the damage detection.

5 Discussions

(a) Concerns on the model-based approach

There are concerns on the feasibility of the proposed approach based on model of the original configuration of the vehicle-bridge system. Not all the original vehicle-bridge systems are available at the time of damage detection. The dynamic properties measured from a real structure at its original configuration may be quite different from those computed from the design drawings of the

structure.

In the process of damage detection, three different models can be developed for the bridge structure, i.e. (a) the original state with the original configuration; (b) the in-service state before damage occurrence; and (c) the damaged state after damage occurrence. Model (a) is usually developed from the design drawings, while models (b) and (c) are obtained from response measurements from field tests.

The proposed approach does not require the dynamic properties obtained from the measured responses of the original configuration (model (a)) as it is usually absent for most structures. The reference model in this model-based damage identification approach is the model at the in-service state (model (b)). The dynamic properties between models (a) and (b) may be quite different due to wear and tear and local modifications made on the structure. The accuracy of reference model (b) can be improved with measured information using a wide range of existing model updating techniques. However, an accurate model of the numerical model is preferable and necessary to facilitate accurate identification results.

The proposed algorithm of damage identification with the objective function in Eq. (11), therefore, refers to the measured data from the present state (model (c)) of the structure and data from the improved reference model (b) above. Early works on damage detection have concluded that incorrect system matrices would lead to smearing of the identified local damage to its adjacent area. With the highly sensitive interaction force studied in this paper, this smearing effect may be reduced but this needs further study in future.

The present model (c), after updating via the proposed method or other techniques with the measured information, it will form the reference model for the next round of damage detection according to the maintenance program of the structure.

(b) Potential problems to be solved for practical application of the proposed method

The methodology proposed in this paper has high potential of application for a quick scan of the large stock of highway bridges with solution to the following problems.

i. Accuracy of the moving sensor - The sensor (vehicle) has to be well-calibrated with instruments. This paper concludes that a slower and heavier vehicle could yield more accurate results. These observations can serve as references in the design of this instrumented vehicle.
ii. Lack of information of the bridge system – General discussions on this problem has been provided in Point (a) above. The connectivity and mass distribution of the bridge system

would be available from the design drawing or from measurement. The system damping can be obtained from preliminary on-site measurement. The boundary conditions are usually well defined and the real conditions can be modeled with unknown constraints for inclusion in the identification of the system together with the unknown local damages. Alternate way to solve the last problem is to include a substructural technique to assess/identify only part of the beam bridge. This could remove this type of uncertainties at the boundaries of the bridge [27].

iii. The unknown road surface roughness – The effect of surface roughness has been extensively studied by many researchers. It is found to be equivalent to the effect of random white noise. Surface roughness of Grades A to D can be properly modeled with defined distributions, while Grade E roughness needs more attention in the identification. However, the latter constitutes only a small group of beam bridges and this problem can be considered later after the trial application of this technique to the bridge structures with other surface roughnesses.

iv. The scenario when there is multiple instrumented vehicles on the beam bridge – The present study involves only a single calibrated instrumented vehicle on the bridge. When multiple instrumented vehicles are involved, the solution of the objective function in Eq. (11) would be benefited with more measured information from the vehicles. Note that the proposed technique does not consider the presence of other vehicles on the beam bridge during test, i.e. the proposed technique requires closure of the bridge in practice.

(c) Possibilities for developing into a full-fledge structural health monitoring (SHM) system for civil infrastructural systems.

The following additional efforts are required before the proposed approach can be generalized into a full-fledge SHM system for civil infrastructural systems.

i. Inclusion of ad-hoc wireless communications with sensors installed on both the bridge and the vehicle;

ii. Development of the smart suspension system of the instrumented vehicle to optimize the excitation imposed on the beam bridge for improved structural health assessment.

6 Conclusions

An innovative idea of utilizing the vehicular interaction forces on top of a beam bridge for damage detection of the structure is presented. A moving sensor in the form of a moving vehicle with two

DOFs is employed for illustration. The interaction force while moving on top of the structure is obtained from the dynamic responses of the vehicle, and the difference between the above-mentioned interaction force and the computed interaction force from the dynamic system serves as an objective function to be minimized with the homotopy iteration algorithm. The following conclusions can be drawn from the simulation studies above:

(1) The vehicle-bridge interaction force along the travelling path of the vehicle is much more sensitive in the detection of local damages in the bridge structure than the acceleration responses from the vehicle axle and body.

(2) The pattern with the vehicle moves at a constant speed across the beam bridge can yield better identified results and with a lower computation cost.

(3) Lower speed and heavier body of the vehicle are recommended as the resulting solution would be less affected by the measurement noise. However, a higher sampling frequency would help to have better accuracy in the identified result.

Acknowledgements

This research is supported by research project funding of the Hong Kong Polytechnic University (G-UB13 and G-YM81), and research funding of the Australian Research Council Discover Project (DP160103197). These financial aids are gratefully acknowledged.

References

[1] W. Fan and P.Z. Qiao, Vibration-based damage identification methods: a review and comparative study. Structural Health Monitoring, 10 (2011) 83-111.

[2] A. Malekjafarian, P.J. McGetrick and E.J. OBrien, A review of indirect bridge monitoring using passing vehicles. Shock and Vibration, 2015 (2015) Article ID 286139.

[3] X.Q. Zhu and S.S. Law, Structural health monitoring based on vehicle-bridge interaction: accomplishments and challenges. Advances in Structural Engineering, 18 (2015) 1999-2015.

[4] Y.B. Yang, C.W. Lin and J.D. Yau, Extracting the bridge frequencies from the dynamic response of a passing vehicle. Journal of Sound and Vibration, 272 (2004) 471–93.

[5] C.W. Lin and Y.B. Yang, Use of a passing vehicle to scan the fundamental bridge frequencies: an experimental verification. Engineering Structures, 27 (2005) 1865-1878.

[6] A. Malekjafarian and E.J. OBrien, Identification of bridge mode shapes using short time frequency domain decomposition of the responses measured in a passing vehicle. Engineering

Structures, 81 (2014) 386-397.

[7] Y.B. Yang and W.F. Chen, Extraction of bridge frequencies from a moving test vehicle by stochastic subspace identification. Journal of Bridge Engineering ASCE, 21 (2015) 04015053.

[8] X. Kong, C.S. Cai, L. Deng and W. Zhang, Using dynamic responses of moving vehicles to extract bridge modal properties of a field bridge. Journal of Bridge Engineering ASCE, 22 (2017) 04017018.

[9] J.Q. Bu, S.S. Law and X.Q. Zhu, Innovation bridge condition assessment from dynamic response of a passing vehicle. Journal of Engineering Mechanics ASCE, 132 (2006) 1372-1379.

[10] C.W. Kim and M. Kawatani, Pseudo-static approach for damage identification of bridges based on coupling vibration with a moving vehicle. Structure and Infrastructure Engineering, 4 (2008) 371-379.

[11] K.-C. Chang, C.-W. Kim and M. Kawatani, Feasibility investigation for a bridge damage identification method through moving vehicle: laboratory experiment. Structure and Infrastructure Engineering, 10 (2014) 328-345.

[12] J. Kim, J.P. Lynch, J.-J. Lee and C.-G. Lee Truck-based mobile wireless sensor networks for the experimental observation of vehicle-bridge interaction. Smart Materials and Structure, 20 (2011) 065009.

[13] F. Cerda, J. Garret, J. Bielak, R. Bhagavatula and J. Kovacevic, Exploring indirect vehicle-bridge interaction for bridge structural health monitoring. Proceedings of the International Conference on Bridge Maintenance, Safety and Management, Philadelphis, PA, USA, (2010) pp. 696-702.

[14] A. Gonzalez, E.J. Obrien and P.J. McGetrick, Identification of damping in a bridge using a moving instrumented vehicle. Journal of Sound and Vibration, 331(2012) 4116-4131.

[15] J. Keenahan, E.J. Obrien, P.J. McGetrick and A. Gonzalez, The use of a dynamic truck-trailer drive-by system to monitor bridge damping. Structural Health Monitoring, 13 (2014) 143-157.

[16] A. Miyamoto and A. Yabe, Bridge Condition Assessment based on Vibration Responses of Passenger Vehicle. Journal of Physics: Conference Series, 305 (2011) 012103.

[17] Y. Zhang, L.Q. Wang and Z.H. Xiang, Damage detection by mode shape squares extracted from a passing vehicle. Journal of Sound and Vibration, 331 (2012) 291-307.

[18] Y. Zhang, S.T. Lie and Z.H. Xiang, Damage detection method based on operating deflection shape curvature extracted from dynamic response of a passing vehicle. Mechanical Systems and Signal Processing, 35 (2013) 238-254.

[19] J.H. He, Homotopy perturbation method: a new nonlinear analytical technique, Applied Mathematics and Computation, 135 (2003) 73-79.

[20] S.J. Liao, On the homotopy multiple-variable method and its applications in the interactions of nonlinear gravity waves, Communications in Nonlinear Science and Numerical Simulation, 16 (2011) 1274-1303.

[21] J.C. Alexander and J.A. Yorke, The homotopy continuation method: numerically implementable topological procedures, Transactions of the American Mathematical Society, 242 (1978) 271-284.

[22] S.H. Choi, D.A. Harney and N.L. Book, A robust path tracking algorithm for homotopy continuation. Comput. Chem. Eng. 20 (1996) 647–655.

[23] K. Iba, H. Suzuki, M. Egawa and T. Watanabe, Calculation of critical loading condition with nose curve using homotopy continuation method. IEEE Trans. Power Syst. 6 (1991) 584–593.

[24] Z.R. Lu and S.S. Law, Features of dynamic response sensitivity and its application in damage identification. Journal of Sound and Vibration, 303 (2007) 305-329.

[25] International Standard Organization (ISO) (1995). Mechanical vibration-Road surface profiles: Reporting of measured data. ISO 8608:1995(E)

[26] D.Y. Zheng, Y.K. Cheung, F.T.K. Au and Y.S. Cheng, Vibration of multi-span non-uniform beams under moving loads by using modified beam vibration functions. Journal of Sound and Vibration, 212 (1998) 455-467.

[27] K. Liu, S.S. Law and X.Q. Zhu, Substructural condition assessment based on force identification and interface force sensitivity. International Journal of Structural Stability and Dynamics, 15 (2015) 1450046.

Table 1: Identified results from different types of responses

Element number	True damage indices	Bu et al. (2006)		Proposed HIA method			
		$\ddot{y}_1$	$\ddot{y}_2$	$\mathbf{P}_{\text{int}}$	$\ddot{y}_{b4}$	$\ddot{y}_1$	$\ddot{y}_2$
1	-5	-5.01	-4.95	-5.003	-5	-5.009	-5.008
2	-10	-9.94	-10.01	-9.999	-9.999	-9.997	-9.996
3	0	-0.13	0	0	-0.002	-0.001	-0.003
4	-10	-9.85	-10	-10	-9.998	-10	-9.998
5	0	-0.21	0	0	0	0	-0.002
6	-15	-14.99	-15	-15	-15	-15	-14.999
7	0	-0.17	-0.01	0	0	0	-0.002
8	0	0.11	0.01	0	0	0	0
9	0	-0.07	-0.02	-0.001	0	0	-0.002
10	0	0.05	0.04	0	-0.007	0	0
AE(%)	-	0.3684	0.0693	0.0033	0.0076	0.0095	0.0103
Iteration number	-	41	37	55	79	136	94

Notes: $\ddot{y}_{b4}$ is the acceleration response of the bridge beam at Node 4.

Table 2: Effect of the vehicle speed and the sampling frequency

Moving speed (m/s)	Sampling frequency (Hz)	Absolute error (%) / Iteration number			
		No noise	2% noise	5% noise	10% noise
1	200	0.00 / 22	1.20 / 86	2.30 / 74	3.75 / 105
4	200	0.00 / 17	13.75 / 78	20.68 / 112	29.67 / 170
4	500	0.00 / 17	4.34 / 81	10.78 / 159	22.12 / 218
4	1000	0.00 / 26	3.11 / 94	6.38 / 128	18.39 / 217
14	200	0.00 / 19	26.19 / 163	38.36 / 229	45.11 / 201

Table 3 - Effect of vehicle mass

Scenarios	vehicle body m_{v1}	Division of homotopy parameter / Iteration number		
		No noise	5% noise	10% noise
1	$3600kg$	10 / 109	20 / 248	20 / 287
2	$3\times3600kg$	15 / 108	20 / 265	20 / 284
3	$5\times3600kg$	10 / 110	20 / 186	20 / 157

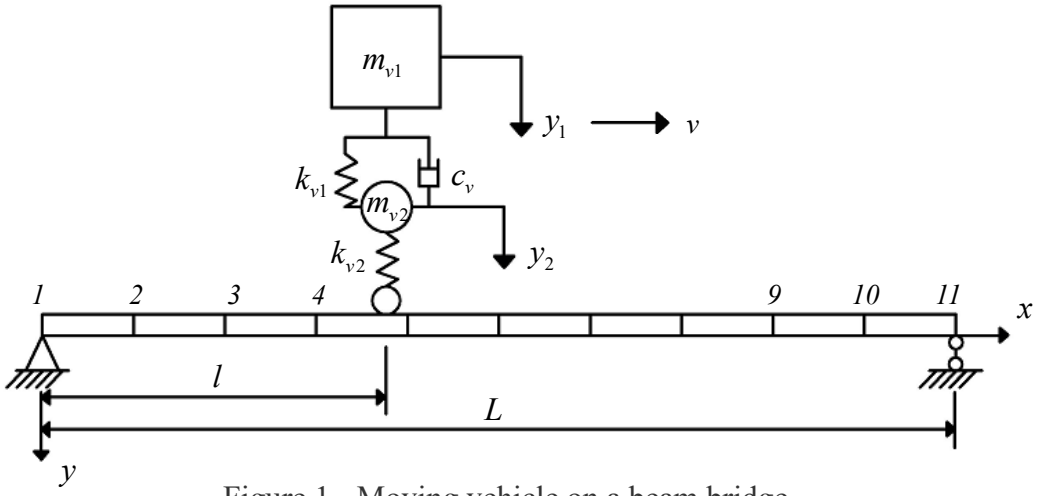

Figure 1 - Moving vehicle on a beam bridge

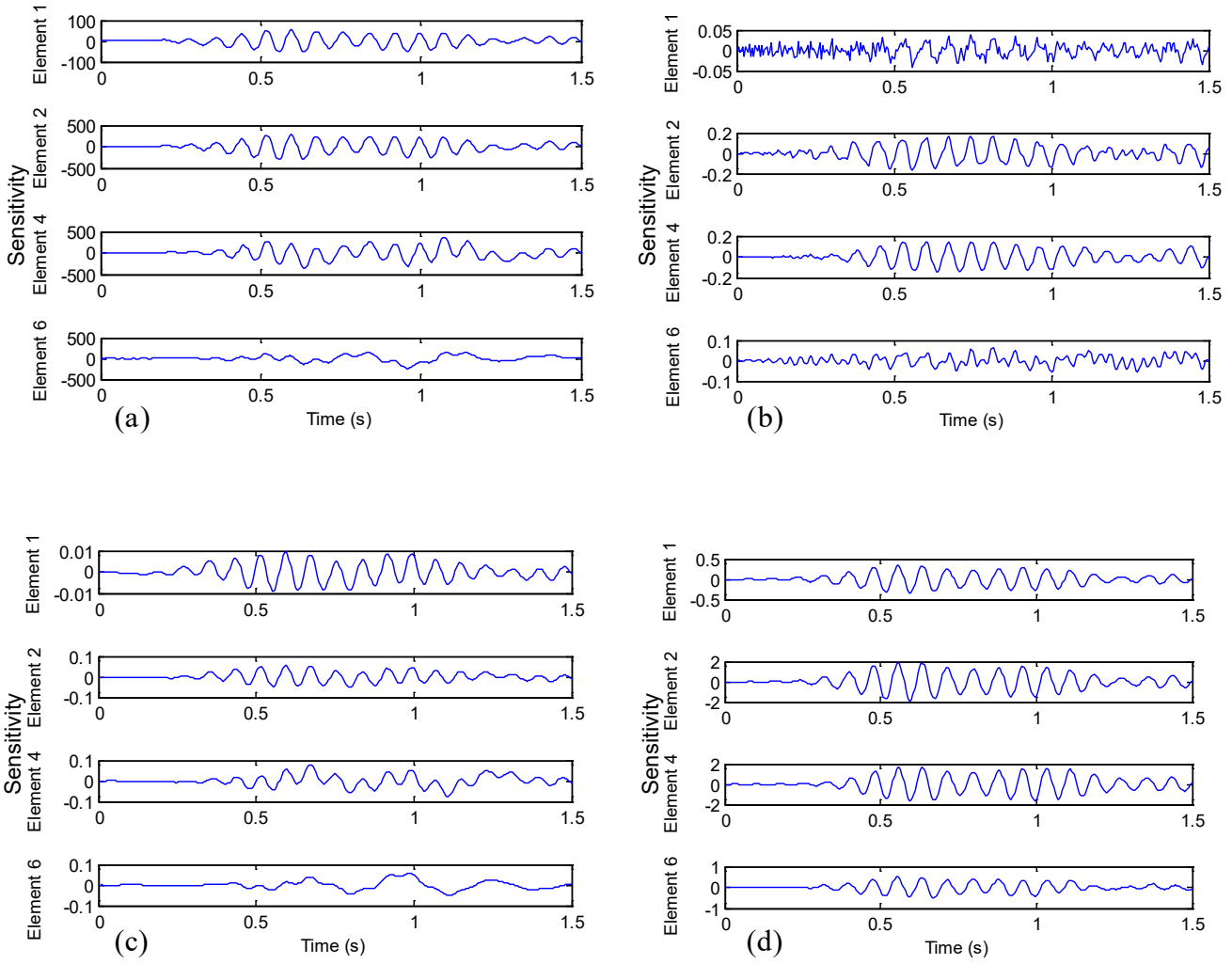

Figure 2 - Different response sensitivities to the damage of different elements: (a) interaction force sensitivity, (b) acceleration sensitivity at Node 4 on the bridge, (c) acceleration sensitivity from the vehicle body mass m_{v1}, (d) acceleration sensitivity from the vehicle axle mass m_{v2}.

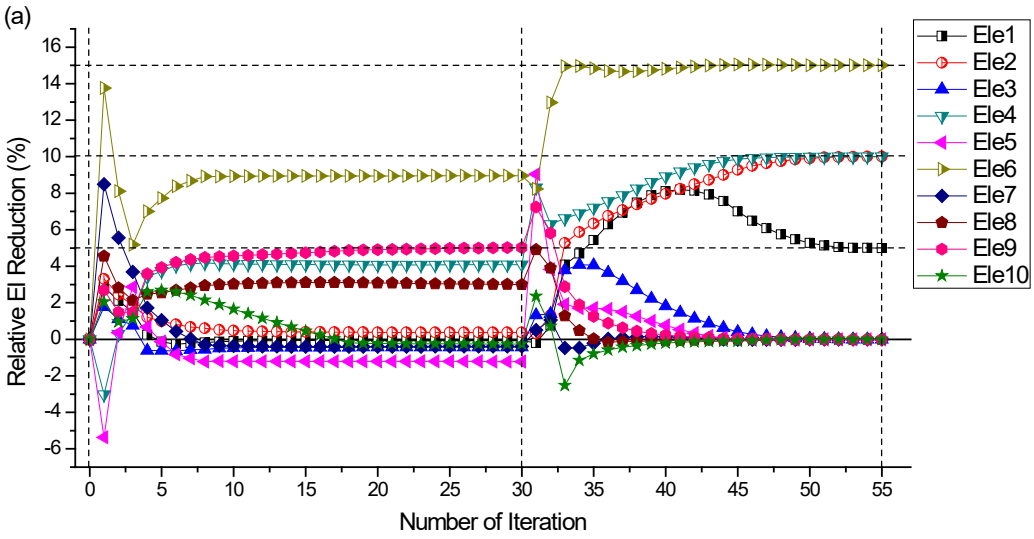

Figure 3(a) - Evolution of identified results from interaction force (satisfying Eq. (19a))

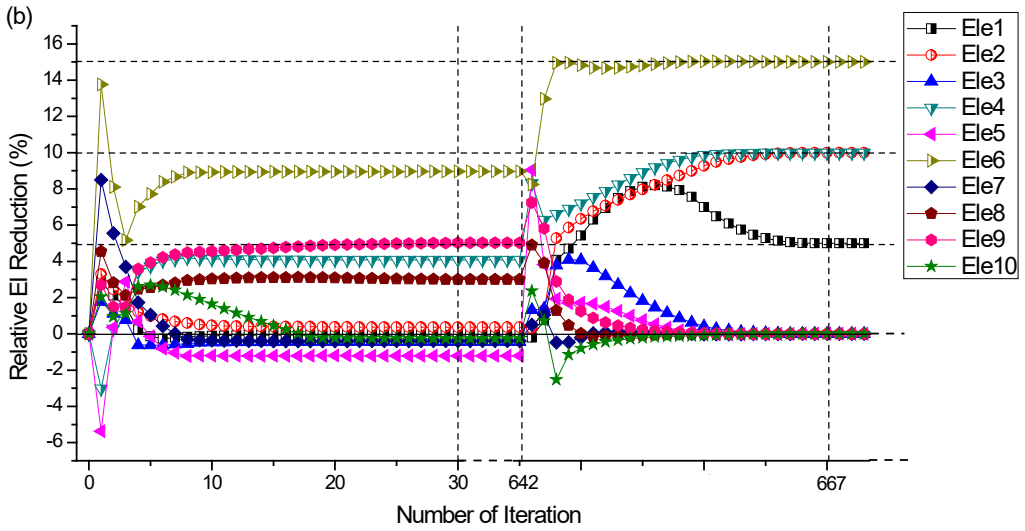

Figure 3(b) - Evolution of identified results from interaction force (satisfying Eqs. (19a) and (19b))

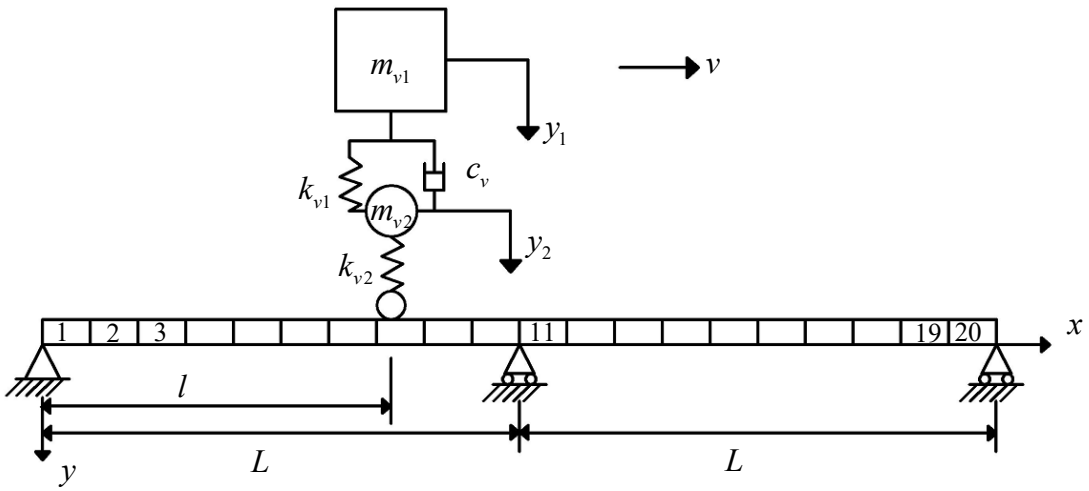

Figure 4 - Moving vehicle in a two-span beam bridge

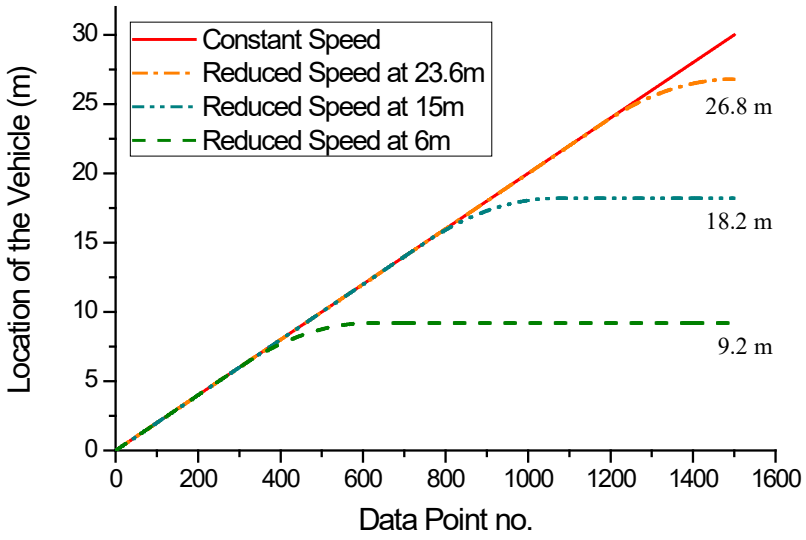

Figure 5 - Moving patterns

(a)

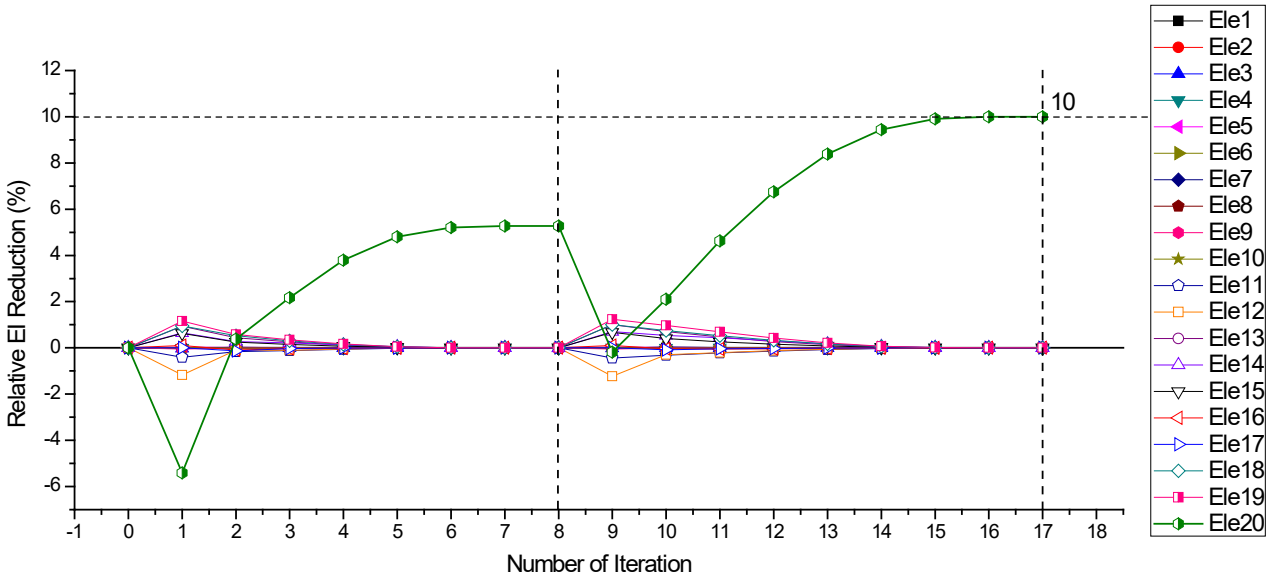

(b)

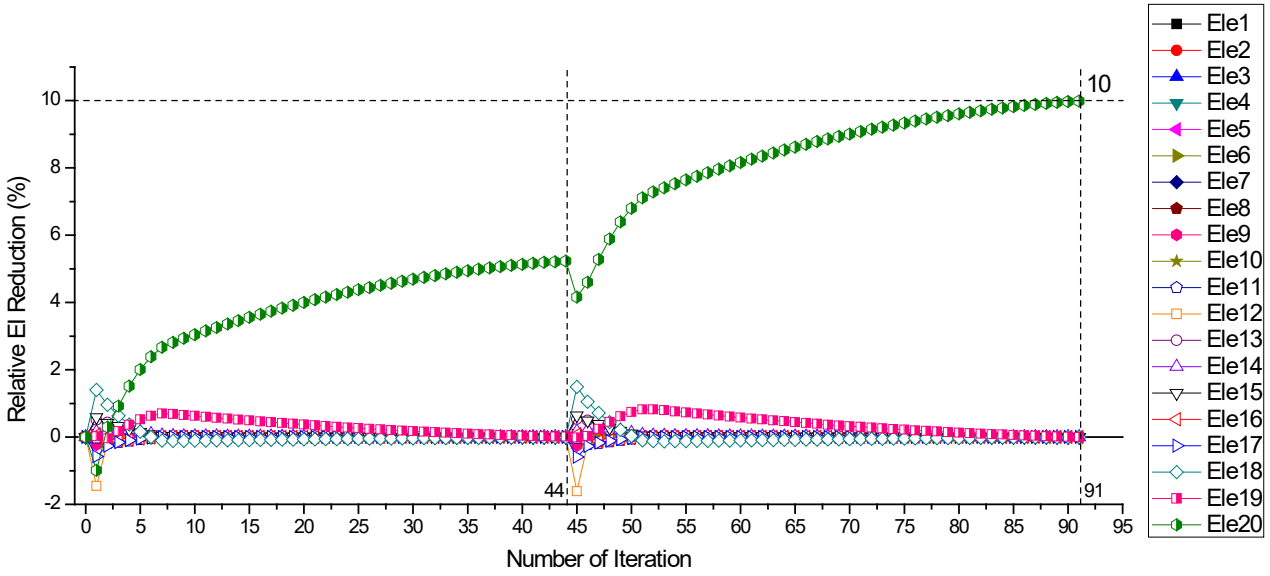

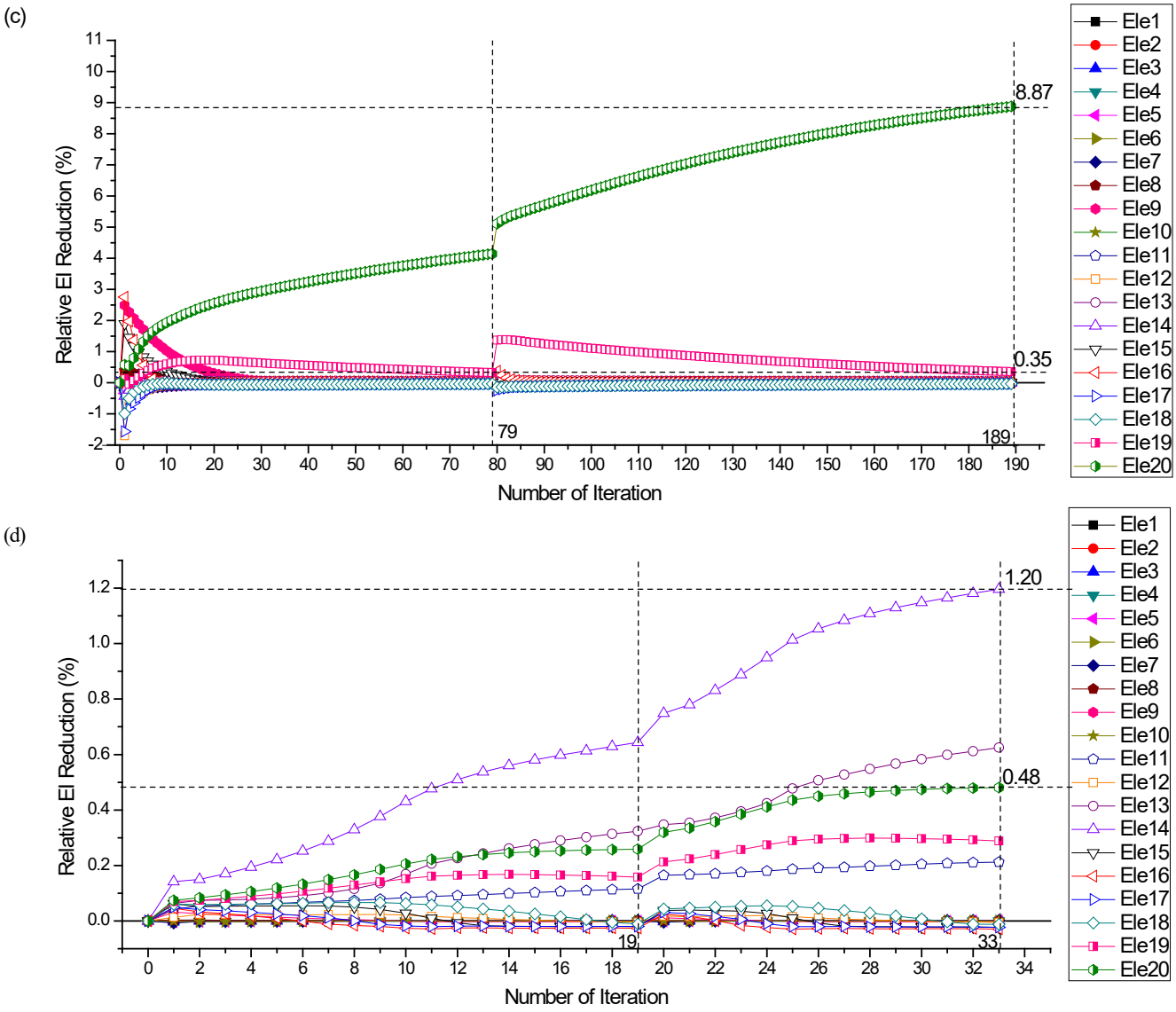

Figure 6 - Identified results under different moving patterns: (a) move at constant 4m/s; (b) decelerates at 23.6m; (c) decelerates at 15m; (d) decelerates at 6m.

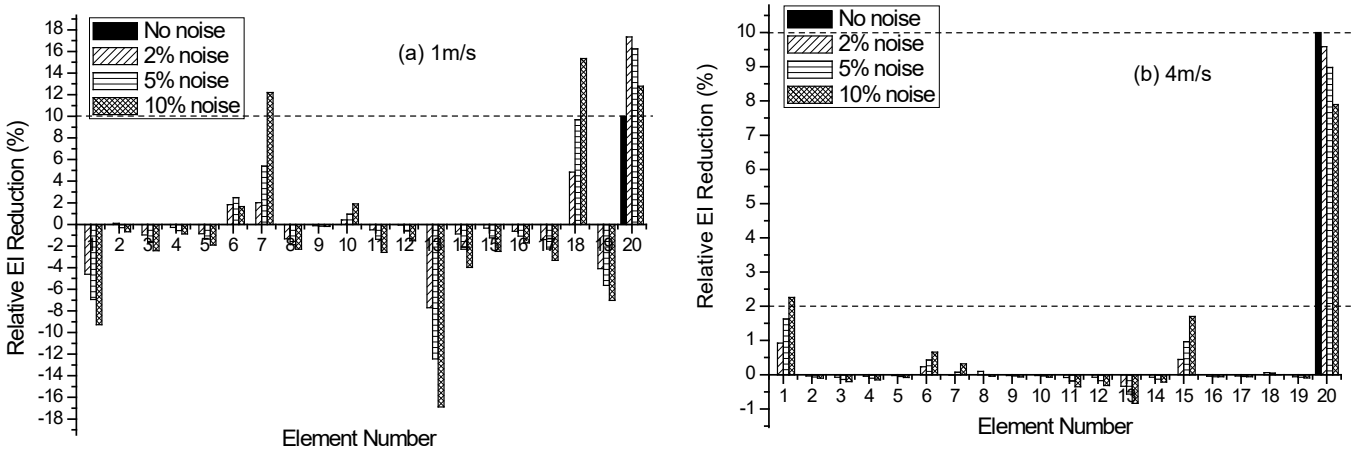

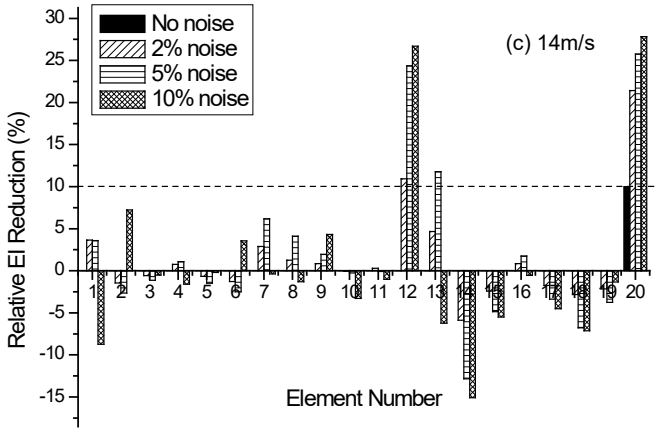

Figure 7 - Identified result from different moving speeds

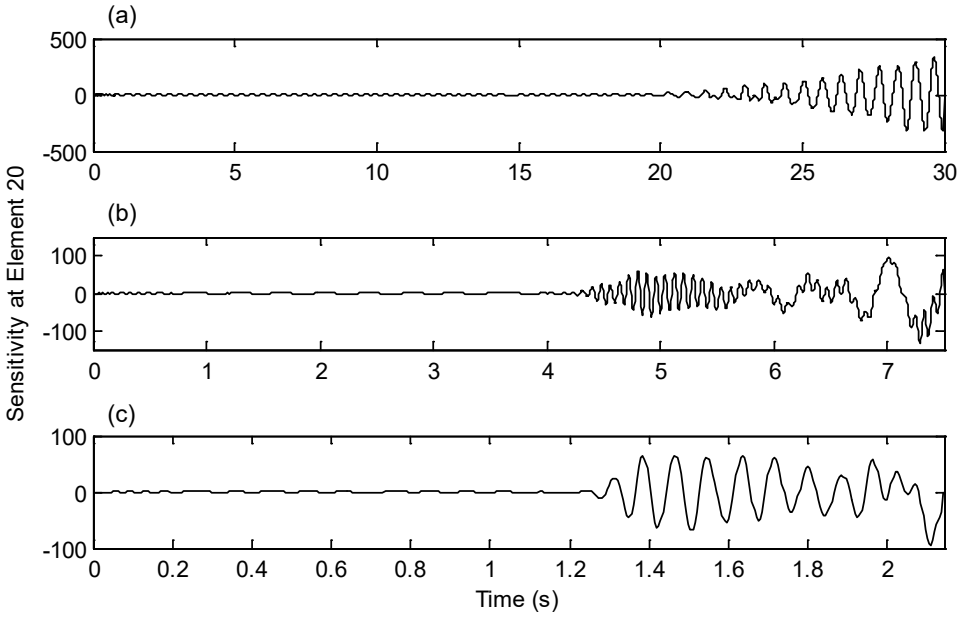

Figure 8 - Sensitivities of interaction force at Element 20 with different moving speeds: (a) 1m/s; (b) 4m/s; (c) 14m/s.

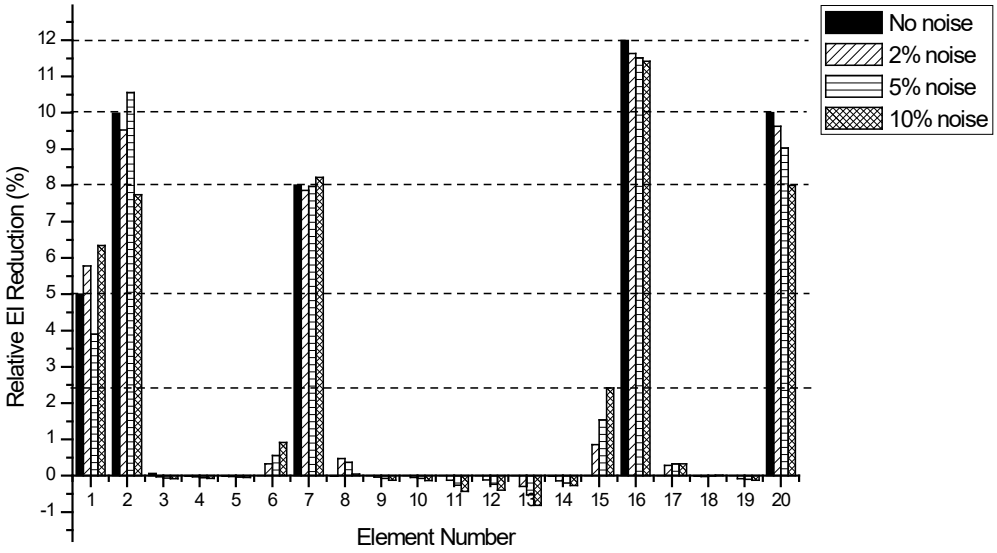

Figure 9 - Identification of multiple damages with different measurement noise

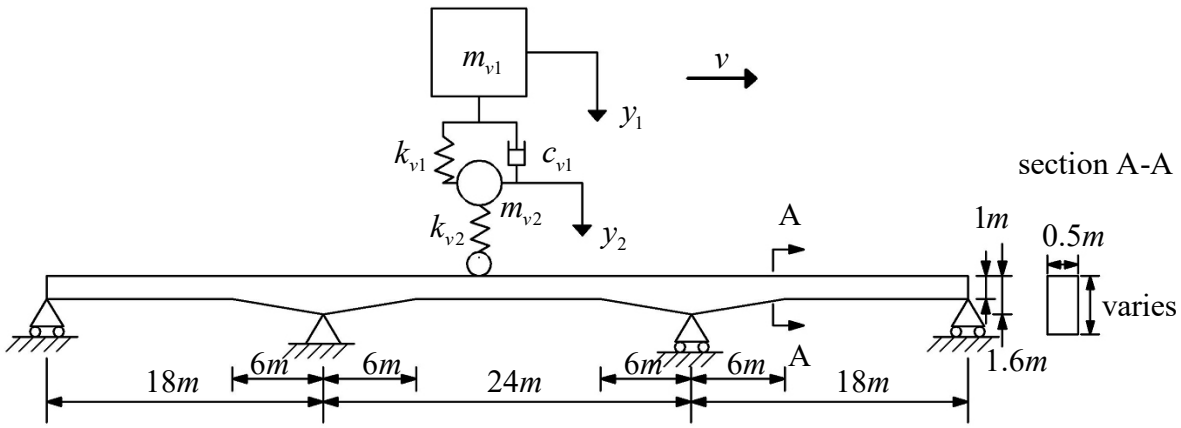

Figure 10 - A three-span continuous haunch beam under a moving vehicle

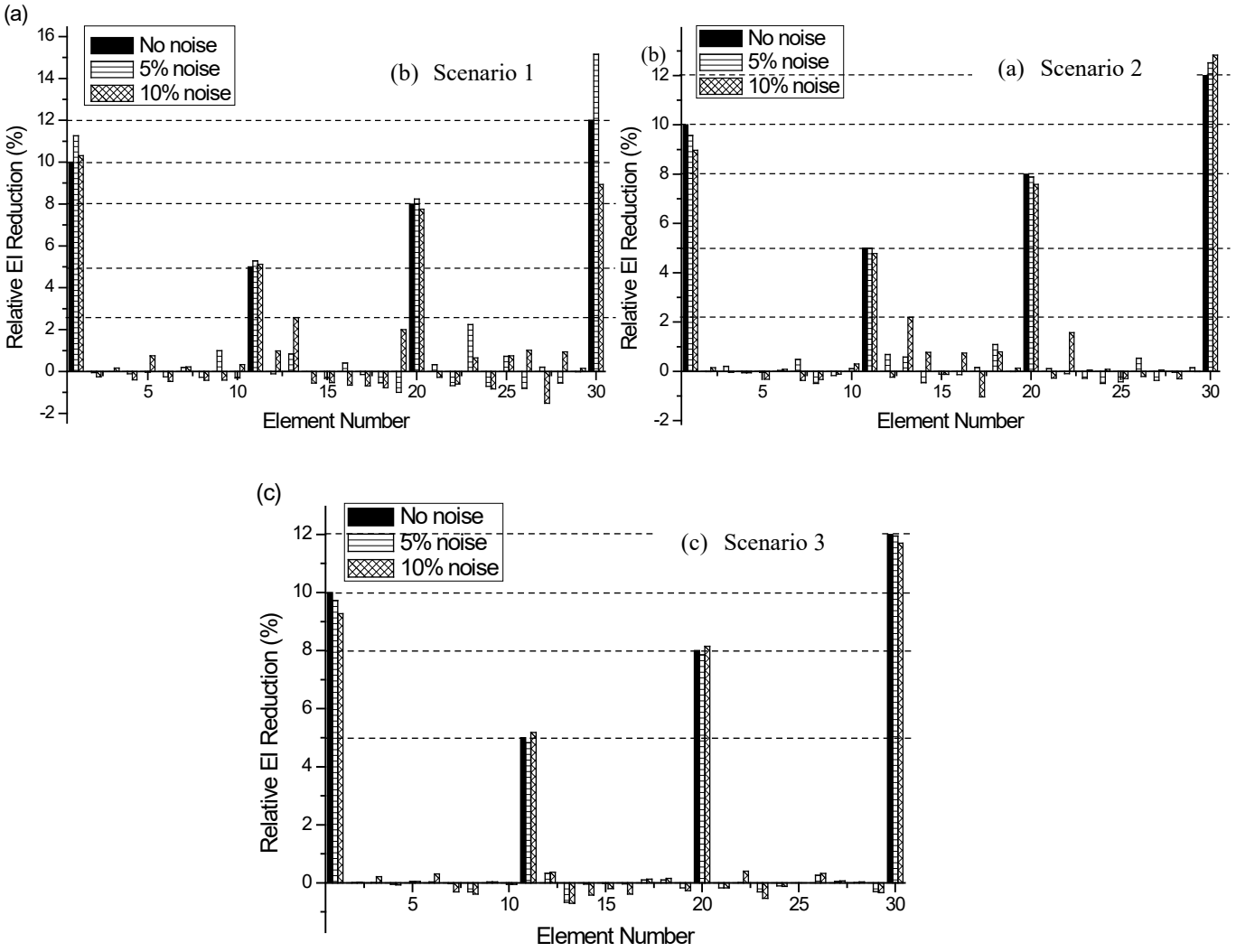

Figure 11 - Identified result